JOURNAL OF SOLID STATE CHEMISTRY 137, 104–111 (1998)
ARTICLE NO. SC977724

Pressure-Induced Phase Transformation of LiIn and LiCd: From NaTl-Type Phases to β-Brass-Type Alloys

U. Schwarz,[1] S. Bräuninger, and K. Syassen

Max-Planck-Institut für Festkörperforschung, Heisenbergstr. 1, D-70569 Stuttgart, Germany

and

R. Kniep

Eduard-Zintl-Institut, Technische Universität Darmstadt, Hochschulstr.10, D-64289 Darmstadt, Germany

Received August 22, 1997; in revised form November 20, 1997; accepted December 4, 1997

We have performed angle-dispersive X-ray powder diffraction experiments on LiGa, LiIn, LiZn, and LiCd at pressures up to 21 GPa using diamond anvil cell techniques. Upon thermal annealing, LiIn and LiCd are both found to undergo phase transformations at a pressure of 11(1) GPa into high-pressure phases with a β-brass (CsCl) structure. Optical reflectivity measurements indicate metallic behavior of the ambient-pressure phases. Band structure calculations for LiIn confirm the covalent character of the bonding within the diamond-type indium partial structure. The transformation into the CsCl-type phase is associated with a loss of directional In–In bonds. © 1998 Academic Press

INTRODUCTION

Zintl phases are polar intermetallic compounds of definite composition with usually anionic partial structures obeying the $(8-N)$ rule of normal valence compounds. The complex mixtures of ionic and covalent bonding properties of Zintl phases have stimulated detailed experimental and theoretical studies (for reviews, see, e.g., refs 1–4), including high-pressure investigations (5–9). We are mainly concerned with LiIn and LiCd, which are classical NaTl-type (10) representatives where the electron-accepting components are located close to the Zintl border (11). Especially LiIn combines the homogeneity range of intermetallic phases with saltlike properties of valence compounds. Describing the chemical bonding in LiIn in accordance with the Zintl–Klemm–Busmann formalism (12–15), it can be assumed that one electron per formula unit is transferred from lithium to the more electronegative indium atom. Then, the In^- anions are isoelectronic with tin and form an α-Sn (diamond-type) partial structure with homonuclear bonds. To describe tetrahedral bonding in LiCd according to the $(8-N)$ rule, participation of one d electron would have to be assumed, resulting in a d^9 configuration for cadmium. Magnetic measurements, however, give no indication of unpaired d electrons (14, 16). Therefore, different bonding properties within the anionic partial structures of LiCd and LiIn are expected.

At ambient conditions, LiIn and LiCd crystallize in face-centered cubic crystal structures which consist of two interpenetrating diamond lattices shifted by $[\frac{1}{2}, \frac{1}{2}, \frac{1}{2}]$ with respect to each other (see Fig. 1a). The first coordination spheres of both atom types are regular cubes which are built from two tetrahedra, each consisting of atoms of the same type. The corresponding lithium compounds of the heavier group homologues, LiTl and LiHg, crystallize in the β-brass structure (CsCl-type), which is shown in Fig. 1b. Here, both types of atoms are coordinated by a cube of unlike atoms. Thus, the crystal structures of the NaTl-type and of the CsCl-type are closely related since they can be viewed as different binary varieties of a bcc arrangement.

The structural and physical properties of intermetallic alkali metal compounds with crystal structures isotypic with CsCl or NaTl have been investigated theoretically by means of band structure calculations (e.g., refs 17–21). Comparing Si and LiAl, for example, calculations reveal similar shapes of the valence electron density within the three-dimensional covalent frameworks (21). In this respect, the original description of the chemical bonding in NaTl-type compounds by Zintl (12, 13) proves to be qualitatively correct. A systematic theoretical investigation (21) shows that the NaTl structure is mainly stabilized by covalent bonds (band structure contributions) whereas the CsCl-type is stabilized by an increase of ionicity (Madelung term). With decreasing volumes, the Madelung energy dominates the band structure

[1] To whom correspondence should be addressed.

0022-4596/98 $25.00

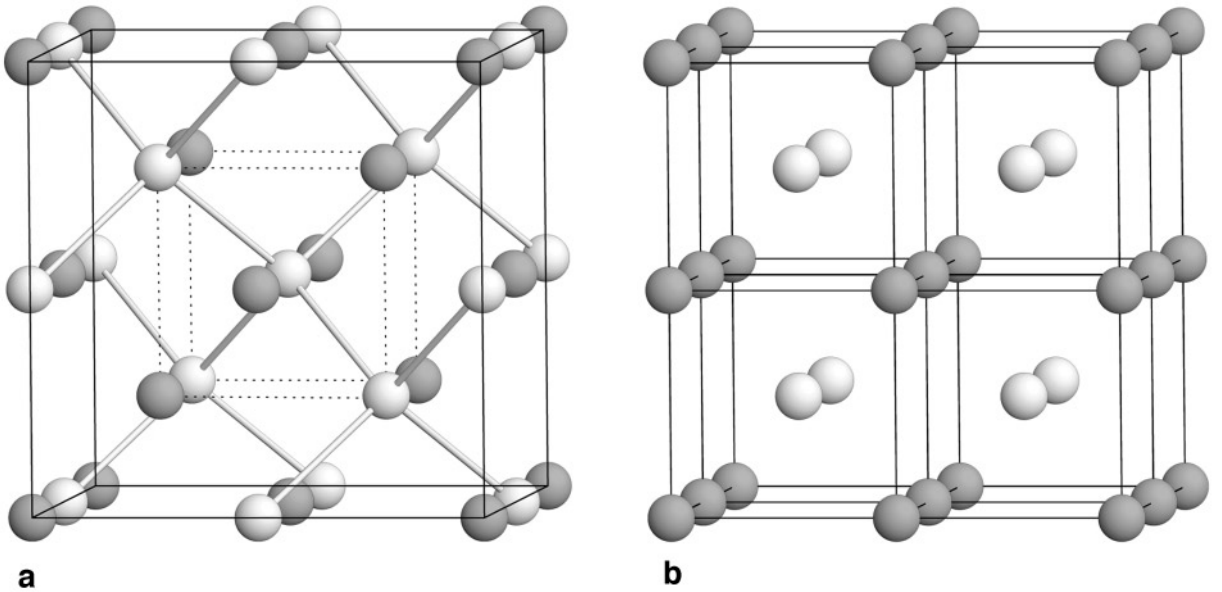

FIG. 1. Ordered binary varieties of a bcc atomic arrangement. (a) NaTl-type crystal structure with one diamond-type partial structure indicated by a ball-and-stick representation. The coordination cube of the central atom is indicated by dotted lines. (b) β-Brass (CsCl-type) structure. Dark atoms, Li; light atoms, In or Cd.

term and the CsCl structure is predicted to become more stable at high pressures (21).

The prediction of pressure-induced structural phase transitions motivated the investigation reported here. We have studied the compressibility and structural stability of LiGa, LiIn, LiZn, and LiCd by means of X-ray powder diffraction at high pressures. It has been shown that the electron localization function (ELF) is a suitable tool to confirm covalent bonding properties, e.g., in diamond-type structures of Group 14 elements (22). Thus, NaTl-type LiIn and LiCd are investigated using calculated electron densities in combination with the ELF to elucidate characteristic differences of the chemical bonding within the polyanionic partial structures. To probe the electronic properties of the compounds experimentally, we performed optical reflectivity measurements.

EXPERIMENTAL

The compounds were synthesized from mixtures of the elements in the molar ratio 1 : 1. The samples were placed in welded Nb ampoules and sealed in silica tubes filled with argon 5.0. Heating to maximum temperatures above the melting point of the 1 : 1 compounds (LiGa: 8 h at 1120 K; LiIn: 8 h at 1020 K; LiZn: 12 h at 920 K; LiCd: 6 h at 970 K) was performed by a chamber furnace. After cooling to ambient temperature at a rate of 10 K/h, the products were characterized by X-ray powder diffraction. Samples were handled under an inert gas atmosphere because of their sensitivity to air and moisture. High pressures were generated with diamond anvil cells (DAC), and chemically inert dried paraffin was used as a pressure-transmitting medium. Pressures were measured by the ruby luminescence method (23). Two different setups were used to collect angle-dispersive X-ray diffraction diagrams. DACs with beryllium backing plates in combination with monochromatic Mo$K\alpha$ radiation and an imaging plate detector system (Molecular Dynamics) were used to collect complete Debye–Scherrer rings. Samples were oscillated by about $\pm 5^\circ$ to improve powder statistics. Integration of the two-dimensional images was performed by means of the program Platypus (24). In experiments involving thermal annealing of the samples, a slit-type DAC and a two-circle diffractometer equipped with a position-sensitive detector was used. Lattice parameters were determined by a least-squares procedure with d-values in the range $140 \leq d \leq 400$ pm. Full profile refinements of the X-ray diagrams were carried out using the program system CSD (25). Optical reflectivity data were collected with a microoptical setup (26). In the reflectivity measurements CsCl was used as a pressure medium to ensure direct optical contact of the freshly cleaved sample chips and the diamond window.

RESULTS

X-Ray Diffraction

Figure 2 shows experimental X-ray powder diffraction data of LiIn at various pressures up to 12.2 GPa. At

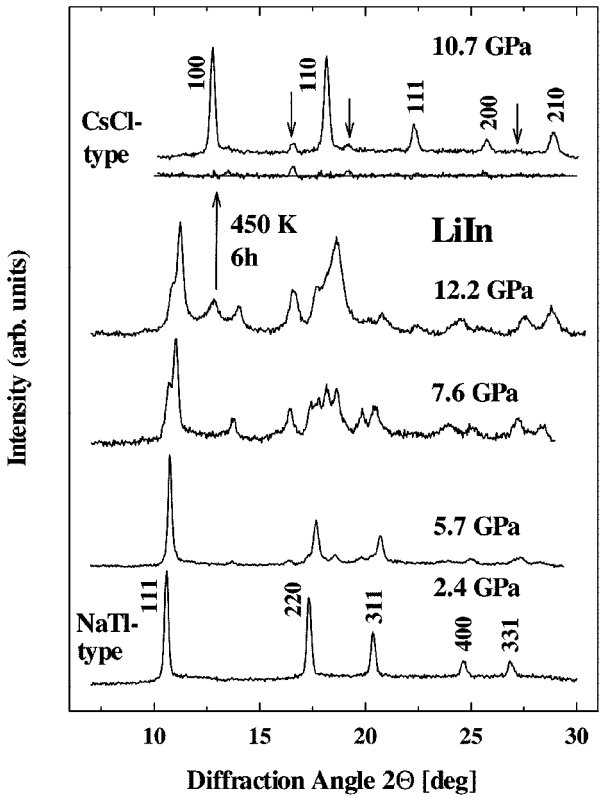

FIG. 2. X-ray powder diffraction diagrams of LiIn. At 2.4 GPa, diffraction data are compatible with a NaTl-type crystal structure ($R_I = 0.042$, $R_{Pr} = 0.18$). The beginning of the phase transformation at 5.5(5) GPa is indicated by additional reflections in the diagram recorded at 5.7 GPa. The patterns at 7.6 and 12.2 GPa illustrate typical changes in the mixed-phase region. After thermal annealing, line positions at 10.7 GPa are consistent with a CsCl-type high-pressure phase ($R_I = 0.011$, $R_{Pr} = 0.145$). Differences between measured and calculated intensities are shown below the experimental data. Arrows indicate weak reflections of $LiIn_3$ (Cu_3Au-type).

TABLE 1
Experimental *d*-Values, Measured and Calculated Intensities, Indices, and Phase Assignment of Diffraction Lines Measured in Direction of Decreasing Pressures at 3.3 GPa[a]

Experimental *d*-value (pm)	Measured intensity	Calculated intensity	Indices	Phase
443.0	33	28	(100)	$LiIn_3$
383.5	83	96	(111)	LiIn
312.5	28	25	(110)	$LiIn_3$
254.8	100	100	(111)	$LiIn_3$
234.4	100	100	(200)	LiIn
220.6	47	51	(200)	$LiIn_3$
199.4	49	54	(311)	LiIn*
199.4	10	15	(210)	$LiIn_3^*$
179.8	10	11	(211)	$LiIn_3$
165.6	14	19	(400)	LiIn
155.5	22	37	(220)	$LiIn_3$
151.8	14	24	(331)	LiIn

[a] Crystallographic data: NaTl-type LiIn, $Fd\bar{3}m$ (space group No. 227), $a = 662.0(3)$ pm, Li at $8a(0,0,0)$, In at $8b(\frac{1}{2},\frac{1}{2},\frac{1}{2})$; Cu_3Au-type $LiIn_3$; $Pm\bar{3}m$ (space group No. 221), $a = 440.4(3)$ pm, Li at $1a(0,0,0)$, In at $3c(0,\frac{1}{2},\frac{1}{2})$. Overlapping reflections at $d \approx 199$ pm are marked with an asterisk. This *d*-value has been omitted from the least-squares refinement of the lattice parameter of $LiIn_3$.

pressures below 5.5(5) GPa, diagrams are consistent with the pure NaTl-type low-pressure form. At higher pressures, the observed transformations of LiIn are quite complex. The appearance of a first set of additional lines is observed at a pressure of 5.5(5) GPa and indicates the onset of a phase transformation. Within the mixed-phase region above 5.5 GPa, the initial NaTl-type LiIn can be identified up to a maximum pressure of 7.0(5) GPa. Within the phase mixture, one phase can be identified by indexing six of the new powder lines assuming a small cubic primitive cell ($a =$ 433 pm at 7.0 GPa). Since attempts to solve the crystal structure using models with 1 : 1 composition failed, a pressure-induced decomposition of LiIn had to be taken into account. A systematic search for cubic alkali metal/alkaline earth metal compounds revealed that Cu_3Au-type $LiAl_3$ (27) is a suitable reference material. A comparison of measured peak intensities and calculated values for $LiIn_3$ with Cu_3Au structure (see Table 1) shows satisfactory agreement. Thus, our X-ray diffraction experiments indicate a decomposition of LiIn at a pressure of 5.5(5) GPa. Attempts to identify the other coexisting phase(s) were not successful. Aiming to obtain single-phase samples of the high-pressure phase, we performed annealing procedures at a temperature of 450 K for typically 12 h. In the pressure range from 6 to 9 GPa, thermal treatment of the samples results in slight reductions of the line widths in the X-ray diagrams but induces no visible changes of relative peak intensities.

At pressures above 11(1) GPa, annealing at a temperature of 450 K for 6 h induces transformation of the phase mixture to a high-pressure phase of LiIn. Line positions and intensities of the strongest lines in the X-ray diagrams (indexed reflections in Fig. 2) are consistent with a CsCl-type crystal structure. Several weak extra lines (marked reflections in Fig. 2) are observed and can be indexed assuming small amounts of Cu_3Au-type $LiIn_3$ ($a = 427.5$ pm at 10.7 GPa). Apparently, pressure induces decomposition first, and further increase helps to stabilize a phase with a 1 : 1 composition again.

The back-transformation of β-brass-type LiIn to a phase mixture is observed at a pressure of 9 GPa. Further decompression leads to the formation of NaTl-type LiIn at 4 GPa. In one series of experiments sample pressures were increased stepwise up to a maximum pressure of 15 GPa, followed by a quick release of pressure down to 3.3 GPa. Under these conditions, the X-ray diagrams indicate coexistence of Cu_3Au-type $LiIn_3$ ($a = 440.4(3)$ pm; see Table 1) and LiIn

with the NaTl structure. Further release of pressure to 0.7 GPa induced the complete back-transformation to NaTl-type LiIn.

In the case of LiCd, the pressure-induced structural transformation proceeds quite differently, as indicated by intensity changes in the X-ray diagrams shown in Fig. 3. With increasing pressure, a continuous intensity decrease of reflections with odd indices (parity group ooo) is observed in NaTl-type LiCd. This effect can be attributed to an increase of disorder among Li and Cd. For a random distribution of both atom types, corresponding to a bcc arrangement, the intensities of reflections with odd indices would become zero. A quantitative determination of occupation factors within the investigated pressure range can be performed by refinements of population parameters G of cadmium using experimental X-ray powder diagrams. We applied the restrictions that the total occupation (cadmium and lithium together) of each Wyckoff position corresponds to one and that the compositions of the samples remain 1 : 1. Figure 4 shows results for the order parameter $\eta = [2 \times G(\mathrm{Cd}) - 1]$ which stem from one series of measurements as a function of pressure. The decrease of η with increasing pressures is small at pressures up to 8 GPa and becomes much more rapid above 8 GPa.

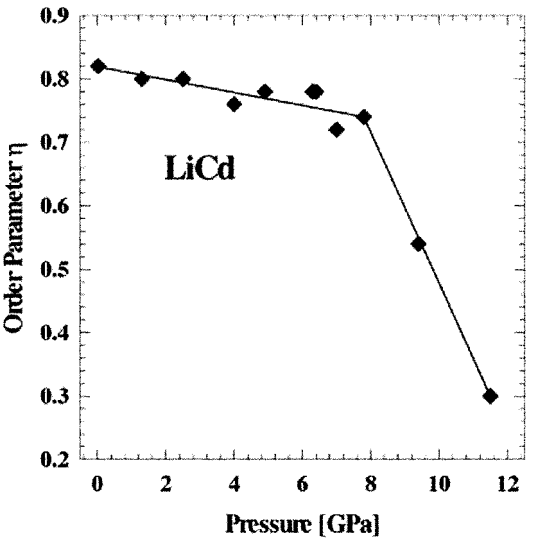

FIG. 4. Order parameter η of the low-pressure modification of LiCd as a function of pressure. The values are obtained from refinements of X-ray powder diffraction diagrams (see text).

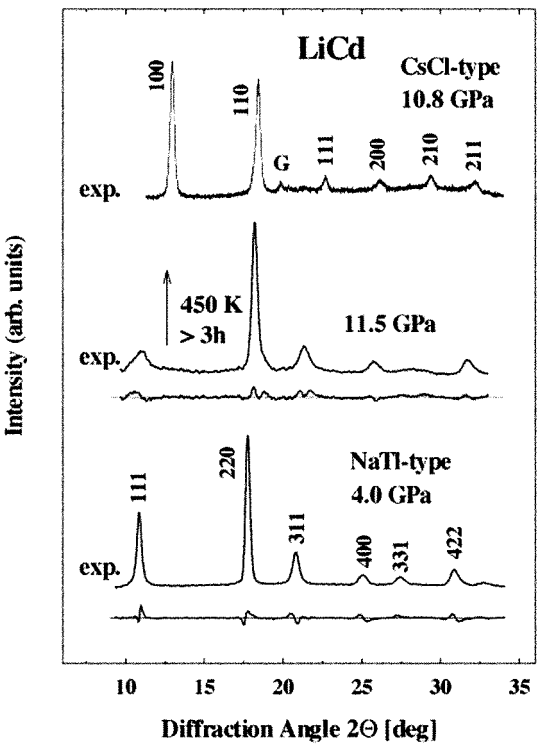

FIG. 3. X-ray powder diffraction diagrams of LiCd. Experimental data at 4.0 and 11.5 GPa are in agreement with a NaTl-type low-pressure form if disorder among cadmium and lithium is considered (see text). Differences between calculated and measured intensities are shown below the diffraction patterns (4.0 GPa: $R_I = 0.038$, $R_{Pr} = 0.150$; 11.5 GPa: $R_I = 0.103$, $R_{Pr} = 0.197$). After a heating procedure, the diagram measured at 10.8 GPa indicates formation of the CsCl-type high-pressure modification ($R_I = 0.057$, $R_{Pr} = 0.235$).

Annealing of almost completely disordered samples at 12 GPa and 450 K for 3 h induces an ordering of the lithium and cadmium atoms into a new phase with a crystal structure of the β-brass-type. In direction of decreasing pressures the phase transformation from the CsCl structure to NaTl-type LiCd takes place without annealing at a pressure of 8 GPa.

Figures 5a and 5b show the pressure–volume data for LiIn and LiCd at pressures up to 18 and 20 GPa, respectively. The solid lines correspond to fits of Murnaghan-type equations of state (28) to the experimental data. The discontinuous changes of volume, which are associated with the structural transformations, are about 3% for LiIn and 5% for LiCd. Bulk moduli of the low-pressure phases of LiIn and LiCd are 39(5) and 43(2) GPa, respectively, assuming a pressure derivative of $B_0' = 4$. Comparison of experimental bulk moduli with values calculated at the theoretical equilibrium volume [LiIn: 34.7 GPa, LiCd: 48.5 GPa (21)] shows reasonable agreement for both compounds. The experimental parameters are close to the values for isoelectronic α-tin [54 GPa (29)] and InSb [46 GPa (30)]. The structural phase transitions into CsCl-type high-pressure modifications are associated with slight increases of the bulk moduli to values of 47(6) and 46(9) GPa for LiCd and LiIn, respectively.

In the case of the homologous compounds LiGa and LiZn, we have not observed any indication of a structural

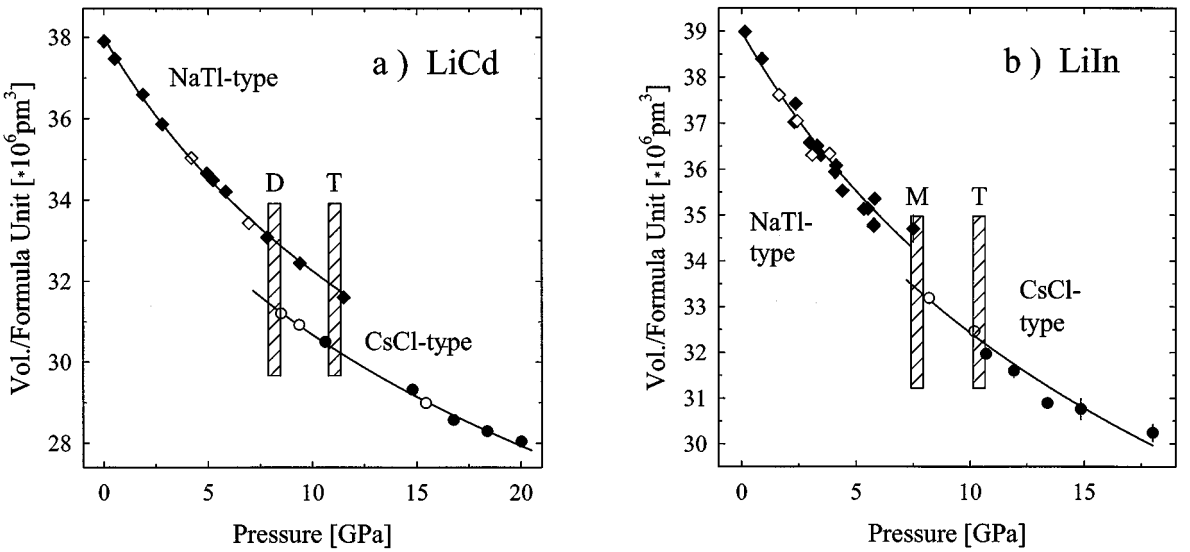

FIG. 5. Pressure–volume relations of (a) LiCd and (b) LiIn. Solid lines correspond to least-squares fits of Murnaghan-type relations (28) to the experimental data. The shaded bars represent the pressures at which (D) the decrease of the order parameter η in LiCd becomes more rapid, (M) NaTl-type LiIn is completely transformed, and (T) transformations to CsCl-type high-pressure phases can be induced by thermal annealing. Filled symbols, increasing pressures; open symbols, decreasing pressures.

change up to a maximum pressure of 21 and 12 GPa, respectively. The experimentally determined bulk moduli of NaTl-type LiGa and LiZn are 71(5) and 40(1) GPa, respectively.

Optical Reflectivity

To obtain information on the electronic properties of the investigated compounds, reflectivity spectra of the low-pressure phases were measured in the energy range from 0.5 to 4 eV (see Fig. 6). All compounds show metal-like behavior at low pressures as indicated by the high reflectivity toward low energies. The Drude-like reflectivity edges of the 1–13 compounds are shifted to lower energies as compared to the 1–12 compounds, a finding which is in accordance with the results of measurements on ternary alloys $LiCd_{1-x}In_x$ ($x = 0.5$–0.3) at ambient conditions (31).

The metallic properties and the positions of the Drude-like edges can be explained by taking into account the different electronic properties as previously calculated (21). The simplified drawings of the band structures in Fig. 7 reveal strong similarities of LiIn to Group 14 semiconductors like Si and Ge. The energy of the "conduction band" drops near the X point of the Brillouin zone below the top of the "valence band," causing semimetallic properties of the binary compounds. The positions of the Drude edges are determined by the onset of direct interband transitions. These are expected to commence at much lower energies in the case of LiIn compared to LiCd (see arrows in Fig. 7) due to different Fermi level positions relative to the top of the valence band region. In accordance with the optical reflectivity data, the calculated band structures of LiGa, LiIn, LiZn, and LiCd indicate metallic behavior.

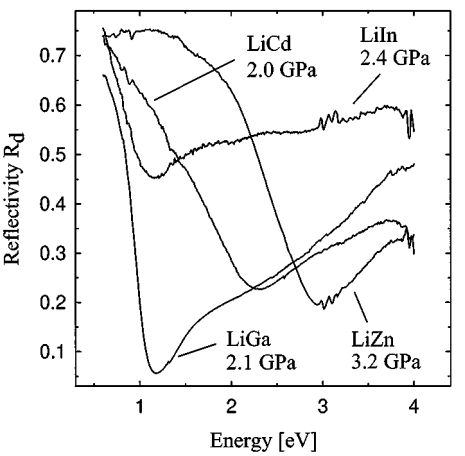

FIG. 6. Optical reflectivity spectra of NaTl-type LiGa, LiIn, LiZn, and LiCd measured in diamond anvil cells. Reflectivity values refer to the absolute reflectivity R_d measured at the interface between sample and diamond window. Common features are high reflectivities at low energies and pronounced Drude-like reflectivity edges.

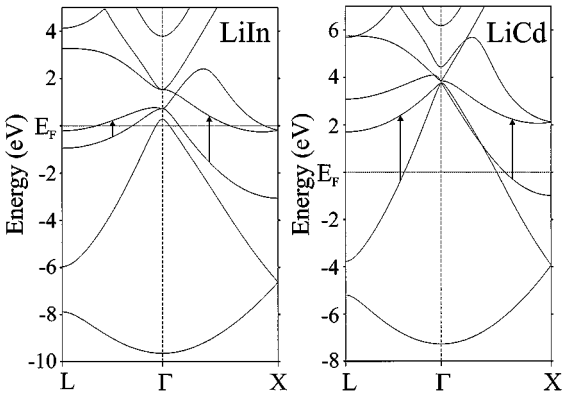

FIG. 7. Band structures of NaTl-type LiIn (left) and LiCd (right) (after ref 21). Several bands crossing the Fermi energy are only partly filled, thus causing semimetallic properties of both compounds.

Calculations

To study the differences in chemical bonding of the low-pressure phases and the changes which are associated with the structural phase transformation from the NaTl-type structure into the CsCl structure, we have investigated the electronic properties of LiIn and LiCd, using calculated electron densities and the electron localization function (ELF) (22, 32). For the purpose of comparing bonding properties within diamond-type frameworks, the corresponding values of α-Sn will be used. We performed calculations within the local density functional approach (LDA) with an exchange correlation potential (33) as implemented in the tight-binding (TB) version (34, 35) of the linear muffin tin orbital (LMTO) (36) Stuttgart-TB-LMTO (37). The basis sets for the one-electron wave functions consisted of five functions (Li 3*s*, 3*p* and 3*d* down-folded (35, 38); In 5*s*5*p*, 5*d* and 4*f* down-folded; Cd 5*s*5*p*, 5*d* and 4*f* down-folded). The calculations include corrections for the neglect of the interstitial region and the higher partial waves (39). The atomic sphere approximation (ASA) requires that the sum of the sphere volumes equals the volume of the unit cell. The resulting wave functions are used to calculate charge densities and the ELF (22, 32) of the valence electrons. The ELF values are normalized so that they cover the range [0, 1]. High values of ELF correspond to low Pauli kinetic energies as can be found in regions of covalent bonds or lone electron pairs.

Figures 8a–d show results of LMTO calculations on α-Sn, LiIn, and LiCd in the form of contour plots in the (110) plane. The upper figures show calculated charge densities and the lower ones ELF values. In Fig. 8a regions of high charge density are found on the short Sn–Sn distances with a maximum valence charge density of 0.32 e/10^6 pm^3. The area between neighboring Sn atoms is characterized by ELF maxima around 0.8, indicating the covalent character of these bonds.

The shape of the charge densities between adjacent In atoms in LiIn (Fig. 8b) exhibits strong similarities to that of α-Sn. As found in the case of Si and LiAl (21), the maximum charge density between neighboring indium atoms of the polyanion is pronouncedly lower (LiIn: 0.21 e/10^6 pm^3) than in the neutral framework of α-tin. Additionally, the absolute ELF values of ≈ 0.7 on the In–In next-neighbor distances (Fig. 8b) are clearly smaller than those of α-Sn. Proceeding to LiCd, we observe drastic changes of the charge density and the ELF, which are shown in Fig. 8c. The homogeneous charge distribution along the Cd zigzag chain and the overall low ELF values between neighboring Cd atoms can be attributed to an increase of metallic character in the Cd–Cd bonds. The weak ELF maximum between adjacent lithium and cadmium atoms is assigned to the polarizing effect of the lithium ions on the valence electrons of the cadmium polyanion. Inspection of the corresponding results for LiIn shows a similar, but less pronounced, feature between lithium and indium. This partly ionic and partly covalent interaction between Li cations and polyanions in NaTl-type Zintl phases is well established and has been discussed in a previous investigation of the compound LiAl (17). Thus, within the series α-Sn, LiIn, and LiCd, we observe the transition from a semiconductor with directional covalent bonds to an intermetallic phase with significantly increased metallic bonding properties within the tetrahedral anion framework.

Figure 8d shows mappings of the valence electron density and the ELF of *β*-brass-type LiIn. The high-pressure phase of LiIn is characterized by a charge distribution around In which shows a distortion from spherical symmetry in the direction of neighboring In atoms. We note here that the distance *d*(In–In) of 312.4 pm (10.8 GPa) is only 6% longer than in NaTl-type LiIn at ambient conditions [294 pm (12, 40, 41)]. Concerning ELF values, local maxima are observed not only between lithium and indium but also halfway between neighboring In atoms, indicating a weak covalent interaction. The decrease of maximum ELF values in the In–In bonds is assigned to a total increase of the metallic character (42) of the high-pressure phase.

CONCLUSIONS

In conclusion, application of hydrostatic pressure causes phase transformations of NaTl-like LiIn and LiCd into high-pressure phases with a *β*-brass (CsCl-type) crystal structure. These transformations proceed along different pathways. For LiIn, we observe a complicated mixed-phase region at pressures above 5.5(5) GPa. One of the products resulting from the pressure-induced decomposition is identified as the hitherto unknown phase $LiIn_3$ with the Cu_3Au

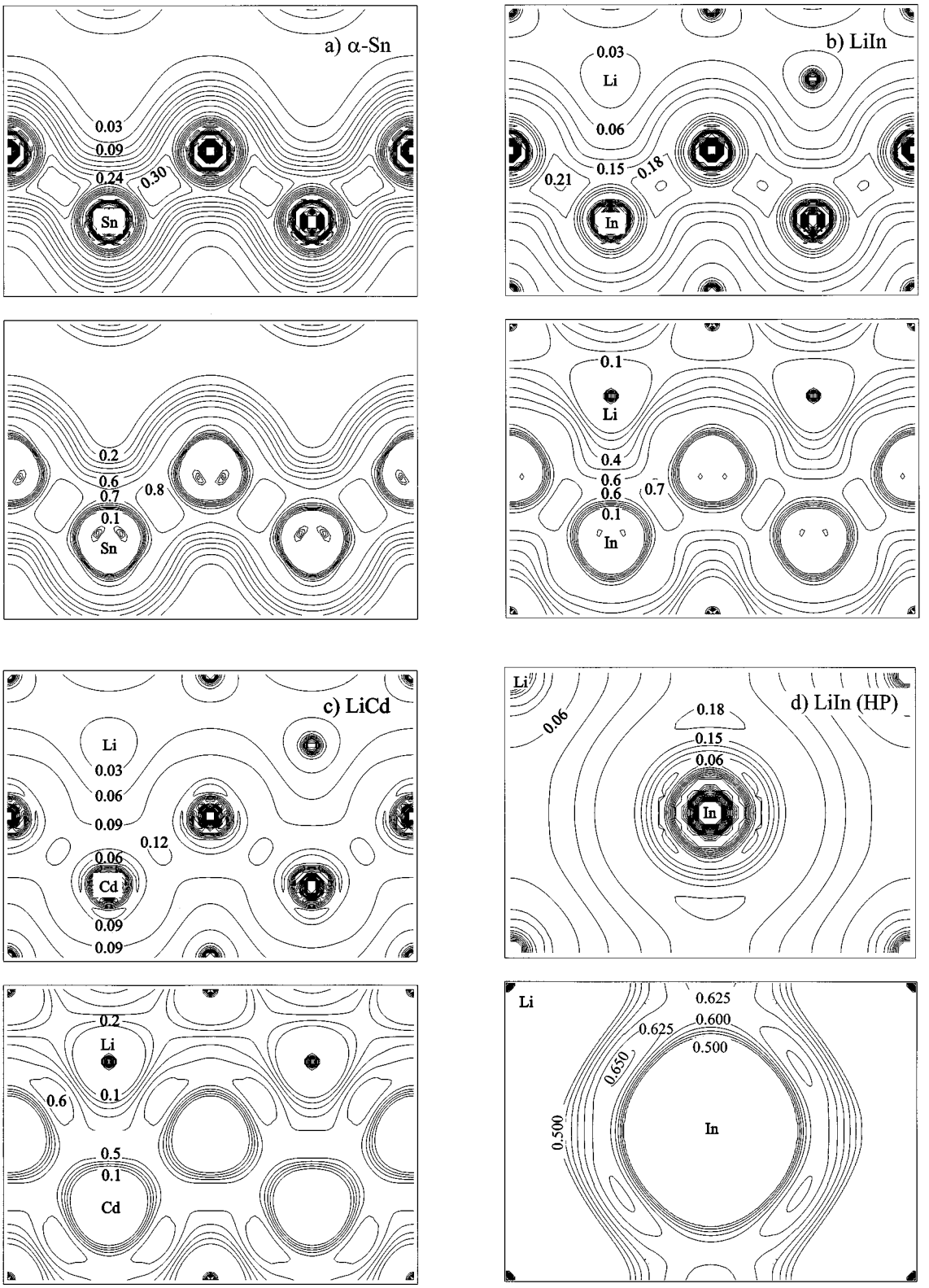

FIG. 8. Calculated charge densities of the valence electrons in $e/10^6$ pm^3 (top) and dimensionless values of the electron localization function (ELF) (bottom) in the (110) plane. Diamond-type structures: (a) α-tin, (b) NaTl-type LiIn, and (c) NaTl-type LiCd. (d) CsCl-type (β-brass) high-pressure form of LiIn.

structure. The phase transformation into a CsCl-type high-pressure phase can be induced by thermal annealing at pressures above 11 GPa. In the case of LiCd, increasing pressure induces disorder of lithium and cadmium atoms. At pressures above 11 GPa, thermal annealing causes ordering of the different atom types into a β-brass-type crystal structure. The experimental observation of CsCl-type high-pressure phases for LiIn and LiCd is consistent with the prediction of previous LMTO calculations (21). The observed structural changes are in accordance with the pressure–homology rule since the heavier homologues of both compounds—LiTl and LiHg—crystallize in the β-brass (CsCl-type) structure at ambient conditions.

Calculations of charge densities and ELF values confirm that the chemical bonding within the In^- partial structure of NaTl-type LiIn is similar to the bonding properties of α-Sn. The finding that the absolute ELF values of the maxima on the In–In next-neighbor distances are smaller than the corresponding values in α-tin is consistent with the results of band structure calculations indicating semimetallic character of the binary compound. Proceeding to LiCd, we observe a significant loss of covalent bonding within the polyanion. The high-pressure phase of LiIn with a β-brass-type structure is characterized by a charge distribution around In which is significantly nonspherical. Evaluation of the ELF reveals local maxima between lithium and indium and in the middle of the distance d(In–In), which are taken as an indication of weak covalent interactions in this intermetallic phase.

REFERENCES

1. H. Schäfer, B. Eisenmann, and W. Müller, *Angew. Chem.* **85,** 742 (1973); *Angew. Chem.*, *Int. Ed. Engl.* **12,** 694 (1973).
2. H. G. von Schnering, *Angew. Chem.* **93,** 44 (1981); *Angew. Chem.*, *Int. Ed. Engl.* **20,** 33 (1981).
3. R. Nesper, *Prog. Solid State Chem.* **20,** 1 (1990).
4. "Chemistry, Structure, and Bonding of Zintl Phases and Ions" (S. Kauzlarich, Ed.). VCH Publishers, New York, 1996.
5. J. Evers, G. Oehlinger, G. Sextl, and A. Weiss, *Angew. Chem.* **96,** 512 (1984); *Angew. Chem.*, *Int. Ed. Engl.* **23,** 528 (1984); *Angew. Chem.* **97,** 499 (1985); *Angew. Chem.*, *Int. Ed. Engl.* **24,** 500 (1985); J. Evers, G. Oehlinger, G. Sextl, and H. O. Becker, *Angew. Chem.* **99,** 69 (1987); *Angew. Chem.*, *Int. Ed. Engl.* **26,** 76 (1987).
6. H. P. Beck and G. Lederer, *Z. Anorg. Allg. Chem.* **619,** 897 (1993).
7. G. Cordier, E. Czech, and H. Schäfer, *Z. Naturforsch.*, *B* **37,** 1442 (1982); *Z. Naturforsch.*, *B* **39,** 421 (1984).
8. J. Evers, G. Oehlinger, and A. Weiss, *Z. Naturforsch.*, *B* **32,** 1352 (1977); *Z. Naturforsch.*, *B* **34,** 524 (1979); *Z. Naturforsch.*, *B* **35,** 397 (1980); *Z. Naturforsch.*, *B* **37,** 1487 (1982); *Z. Naturforsch.*, *B* **38,** 899 (1983); *Angew. Chem.* **89,** 673 (1977); *Angew. Chem.*, *Int. Ed. Engl.* **16,** 659 (1977); *Angew. Chem.* **90,** 562 (1978); *Angew. Chem.*, *Int. Ed. Engl.* **17,** 538 (1978).
9. J. Evers and A. Weiss, *J. Solid State Chem.* **20,** 173 (1977); J. Evers, *J. Solid State Chem.* **24,** 199 (1978); *J. Solid State Chem.* **28,** 369 (1979); *J. Solid State Chem.* **32,** 77 (1980).
10. E. Zintl and W. Dullenkopf, *Z. Phys. Chem. B* **16,** 195 (1932).
11. F. Laves, *Naturwissenschaflen* **29,** 241 (1941).
12. E. Zintl and G. Brauer, *Z. Phys. Chem. B* **20,** 245 (1933).
13. E. Zintl, *Angew. Chem.* **52,** 1 (1939).
14. W. Klemm and H. Fricke, *Z. Anorg. Allg. Chem.* **282,** 162 (1955).
15. E. Busmann, *Z. Anorg. Allg. Chem.* **313,** 90 (1961).
16. Y. L. Yao, *Trans. Metall. Soc. AIME* **230,** 1725 (1964).
17. A. Zunger, *Phys. Rev. B* **17,** 2582 (1978).
18. T. Asada, T. Jarlborg, and A. J. Freeman, *Phys. Rev. B* **24,** 510 (1981).
19. P. C. Schmidt, *Phys. Rev. B* **31,** 5015 (1985).
20. P. C. Schmidt, *Z. Naturforsch.*, *A* **40,** 335 (1985).
21. N. E. Christensen, *Phys. Rev. B* **32,** 207 (1985).
22. A. Savin, A. D. Becke, J. Flad, R. Nesper, H. Preuss, and H. G. von Schnering, *Angew. Chem.* **103,** 421 (1991); *Angew. Chem.*, *Int. Ed. Engl.* **30,** 409 (1991); A. Savin, O. Jepsen, J. Flad, O. K. Andersen, H. Preuss, and H. G. von Schnering, *Angew. Chem.* **104,** 186 (1992); *Angew. Chem.*, *Int. Ed. Engl.* **31,** 187 (1992).
23. H. K. Mao, J. Xu, and P. M. Bell, *J. Geophys. Res.* **91,** 4673 (1986).
24. R. J. Nelmes, P. D. Hatton, M. I. McMahon, R. O. Piltz, J. Crain, R. J. Cernik, and G. Bushnell-Wye, *Rev. Sci. Instrum.* **63,** 1039 (1992); R. O. Piltz, M. I. McMahon, J. Crain, P. D. Hatton, R. J. Nelmes, R. J. Cernik, and G. Bushnell-Wye, *Rev. Sci. Instrum.* **63,** 700 (1992).
25. L. G. Akselrud, Yu. Grin, V. K. Pecharsky, P. Yu. Zavaliy, and V. S. Fundamenskiy, Computer Program CSD 4.10, STOE & Cie, Darmstadt, 1992.
26. R. Sonnenschein and K. Syassen, *Rev. Sci. Instrum.* **53,** 644 (1982).
27. T. Yoshi-Yama, K. Hasebe, and M. Mannami, *J. Phys. Soc. Jpn.* **25,** 908 (1968).
28. F. D. Murnaghan, *Proc. Natl. Acad. Sci. U.S.A.* **30,** 244 (1944).
29. C. J. Buchenauer, M. Cardona, and F. H. Pollak, *Phys. Rev. B* **3,** 1243 (1971).
30. I. O. Baskin and G. I. Peresade, *Sov. Phys. Solid State* **16,** 2058 (1975).
31. M. Zwilling, P. C. Schmidt, and A. Weiss, *Appl. Phys.* **16,** 255 (1978).
32. J. Becke and K. E. Edgecombe, *J. Chem. Phys.* **92,** 5397 (1990).
33. U. Barth and L. Hedin, *J. Phys. C* **5,** 1629 (1972).
34. O. K. Andersen and O. Jepsen, *Phys. Rev. Lett.* **53,** 2571 (1984).
35. O. K. Andersen, O. Jepsen, and D. Glötzel, *in* "Highlights of Condensed-Matter Theory" (F. Bassani, F. Fumi, and M. P. Tossi, Eds.). North-Holland, New York, 1985.
36. O. K. Andersen, *Phys. Rev. B* **12,** 3060 (1975).
37. G. Krier, M. van Schilfgaarde, O. Jepsen, A. Burkhardt, and O. K. Andersen, Computer Program Stuttgart-TB-LMTO.
38. W. R. L. Lambrecht and O. K. Andersen, *Phys. Rev. B* **34,** 2439 (1986).
39. O. K. Andersen, Z. Pawlowska, and O. Jepsen, *Phys. Rev. B* **34,** 5253 (1986).
40. W. A. Alexander, L. D. Calvert, R. H. Gamble, and K. Schinzel, *Can. J. Chem.* **54,** 1052 (1976).
41. T. S. Huang and J. O. Brittain, *Mater. Sci. Eng.* **93,** 83 (1987).
42. U. Häussermann, S. Wengert, P. Hofmann, A. Savin, O. Jepsen, and R. Nesper, *Angew. Chem.* **106,** 2147 (1994); *Angew. Chem.*, *Int. Ed. Engl.* **33,** 2069 (1994).